Results in Engineering 29 (2026) 108664

Contents lists available at ScienceDirect

Results in Engineering

journal homepage: www.sciencedirect.com/journal/results-in-engineering

Surface functionalization of optical fibers with PDDA-stabilized AuNPs for enhanced interfacial stability in sensing applications

Ratchawi Jammee [a], Pannathorn Jitpratak [b], Abinash Panda [c], Paris Uerchuchai [d], Parinthorn Trakarnvanich [e], Akhilesh Kumar Pathak [f], Charusluk Viphavakit [a,*]

[a] International School of Engineering, Biomedical Materials and Devices for Revolutionary Integrative Systems Engineering Research Unit (BMD-RISE), Faculty of Engineering, Chulalongkorn University, Bangkok, Thailand
[b] Biomedical Engineering Program, Faculty of Engineering, Chulalongkorn University, Bangkok 10330, Thailand
[c] Department of Electronics and Communication Engineering, CMR Institute of Technology, Bengaluru, India
[d] Molecular Science and Engineering Program, School of Engineering Sciences in Chemistry, Biotechnology and Health, KTH Royal Institute of Technology, Stockholm, Sweden
[e] Department of Chemistry, Faculty of Science, Chulalongkorn University, Bangkok, Thailand
[f] Department of Mechanical Engineering, Center for Smart Structures and Materials (CSSM), Northwestern University, Evanston, IL, USA

ARTICLE INFO

Keywords:
Gold nanoparticles
Poly(diallyldimethylammonium chloride) (PDDA)
Optical fiber sensor
Ammonia detection
Localized surface plasmon resonances (LSPR)

ABSTRACT

Ammonia sensing is important for environmental monitoring, industrial safety, and food spoilage detection, but achieving a stable and reliable sensing response at low concentrations remains challenging. This work reports the development and optimization of a gold nanoparticle (AuNP) layer stabilized with poly(diallyldimethylammonium chloride) (PDDA) for application in optical fiber ammonia sensing. To optimize the coating process, PDDA concentrations (0.5, 0.10, and 1 wt%), molecular weights (low and medium), and AuNP deposition times (5–20 min) were systematically varied. The optimum condition, identified as 1 wt% medium-molecular-weight PDDA with a 20 min AuNP deposition, produced uniform nanoparticle coverage, enhanced interfacial stability, and a strong plasmonic response. The homogeneous distribution and surface coverage of AuNPs, as well as the adsorption of NH_3 at the AuNP/PDDA interface, were verified by FE-SEM, AFM, and FTIR. The optimized layer was applied onto an optical fiber to demonstrate its structural stability and practical sensing capability, exhibiting concentration-dependent spectral shifts upon NH_3 exposure at 0.5, 1, 5, 10, 15, 20, and 25 ppm under room temperature conditions. A sensitivity of 0.023 nm/ppm with excellent linearity ($R^2 = 0.97$) was achieved, and nitrogen-assisted desorption enabled repeatable operation. This study demonstrates that systematic material optimization provides a stable, uniform, and robust interfacial layer, supporting the potential of the AuNP/PDDA-coated optical fiber for real-world ammonia detection in environmental, industrial, and healthcare applications.

1. Introduction

Volatile organic compounds (VOCs) are abundant chemicals found in consumer products, including cosmetics, paints, and wood floors. Human exposure to VOCs indoors is higher than outdoors, and prolonged exposure has been associated with the development of long-term health effects [1–3]. According to the Environmental Protection Agency, prolonged exposure to specific VOCs has been associated with respiratory irritation, headaches, and an increased risk of certain cancers [2,4]. Among the various VOCs, ammonia is particularly concerned due to its widespread use and significant health risks. Ammonia is a colorless, toxic, and highly versatile organic chemical gas with various industrial, agricultural, and pharmaceutical applications [5]. Exposure to ammonia poses a significant life threat to human health even at low concentrations. The Occupational Safety and Health Administration (OSHA) has established guidelines for maximum ammonia permissible exposure levels in workplace environments [6]. The recommended maximum working exposure time is 8 h with a dose limit of 25 ppm. At higher concentrations, the permissible exposure duration is substantially shorter. Hence, a safe and effective device for accurate and reliable monitoring of ammonia concentration in working environments is critically important. Various sensing materials, such as metal oxides,

* Corresponding author.
E-mail address: charusluk.v@chula.ac.th (C. Viphavakit).

https://doi.org/10.1016/j.rineng.2025.108664
Received 13 October 2025; Received in revised form 2 December 2025; Accepted 8 December 2025
Available online 9 December 2025

polymers, and nanomaterials, have been developed to detect ammonia efficiently in workplace environments [7–11].

To address these detection requirements, researchers have investigated numerous sensing technologies, in which optical fiber-based sensors have emerged as a highly promising approach. Optical fiber-based sensors have gained significant attention in chemical and gas sensing applications due to several advantages, including their lightweight structure, capability for remote sensing in hazardous environments, resistance to electromagnetic interference, and high sensitivity to low analyte concentrations [12–18]. These features make optical fiber sensors suitable for detecting volatile organic compounds, including ammonia. The operating principle of these sensors involves modulating specific properties such as intensity, wavelength, or phase of the light transmitted through the fiber when exposed to particular chemicals or analytes in the surrounding environment [16]. To further enhance sensitivity and selectivity, the surface of the optical fiber is typically functionalized with materials specifically designed to interact with targeted analytes. Recently, the integration of nanotechnology with optical fiber platforms has opened novel pathways, significantly improving the performance and versatility of chemical sensing systems [19–21].

One promising approach is the integration of noble metal nanoparticles, especially gold nanoparticles (AuNPs), which are well known for their unique optical properties and biocompatibility [22–25]. These AuNPs exhibit a strong surface oscillation of conduction electrons at their surface under light excitation, known as localized surface plasmon resonance (LSPR) [26]. LSPR is the collective oscillation of conduction electrons in the nanoparticles, induced by incident light at a specific wavelength. The resonance condition is highly sensitive to changes in the local refractive index at the surface of nanoparticles [27]. The resulting resonance possesses a characteristic wavelength that is sensitive not only to the intrinsic properties of the nanoparticle, such as its size and shape, but also to small changes in the surrounding environment [28]. Realizing the potential of LSPR in practical applications depends on achieving a uniform distribution, controlled orientation, and long-term stability of AuNPs on the substrate. Uncontrolled aggregation can reduce the plasmonic response. Recently, several LSPR fiber biosensors have combined tapered or multicore fiber structures with hybrid nanomaterials, such as double S-tapered probes coated with AuNPs and inorganic functional materials for biomarker sensing applications [29, 30]. These designs achieve high sensitivity by enhancing the evanescent field through the use of complex fiber geometries and multilayer nanocomposites.

The challenges in the fabrication of functional materials, such as AuNPs, involve developing surface techniques to achieve stable and uniform nanoparticle immobilization. Self-assembled monolayers (SAMs) are widely used for AuNP immobilization and offer well-defined surface chemistry. However, their performance can be influenced by subtle variations in silanization conditions, which may affect coating uniformity, especially on small-radius optical fibers [31–33]. Depositing plasmonic colloidal particles directly on transparent silica-based substrates, such as optical fibers, raises major concerns regarding particle instability, as they often aggregate and lose their optical properties [34, 35]. This instability is observed from a dramatic change in the LSPR band due to particle aggregation during the drying process. To overcome this issue, the integration of colloidal nanoparticles with polymer-coated glass substrate is a notable strategy to enhance the stability and functionality of the particles [36,37].

In this work, an optimized AuNP/PDDA layer is proposed as a functional coating for optical fibers to enable stable plasmonic interfaces with sensing capability. The approach employs poly(diallyldimethylammonium chloride) (PDDA) as a cationic polyelectrolyte to immobilize citrate-stabilized AuNPs through electrostatic interactions, thereby preventing aggregation and preserving their optical properties. The effects of PDDA concentration, molecular weight, and AuNP deposition time were systematically investigated to obtain conditions for uniform nanoparticle coverage, stable immobilization, and a strong plasmonic response. The chemical interactions between NH_3 molecules and the AuNP/PDDA layer were included in this study. The optimized layer was subsequently applied onto optical fibers and tested for ammonia detection at concentrations ranging from 0.5 to 25 ppm under room temperature conditions. The sensing performance was evaluated through transmittance spectra and resonance wavelength shifts, with sensitivity and repeatability assessed. This study establishes an optimized AuNP/PDDA layer as a functional material enabling practical optical fiber sensing for ammonia monitoring in environmental, industrial, and healthcare applications.

2. Experimental details

2.1. Materials

All chemicals and reagents were of analytical grade and used without further purification. Gold (III) chloride trihydrate ($HAuCl_4 \bullet 3H_2O$, Sigma-Aldrich, USA) and trisodium citrate dihydrate ($Na_3C_6H_5O_7 \bullet 2H_2O$, KemAus, Cherrybrook, NSW, Australia) were used as precursors for the synthesis of gold nanoparticles (AuNPs). (3-aminopropyl)triethoxysilane ($SiC_9H_{23}NO_3$, APTES) (Sigma-Aldrich, USA), potassium hydroxide pellets (KOH, Merck KGaA, Germany), and low ($M_w < 100$ kDa, 30 wt% in H_2O) and medium ($M_w = 200$ kDa-300 kDa, 20 wt% in H_2O) molecular weight poly(diallyldimethylammonium chloride) solutions (PDDA, Sigma Aldrich, USA) were used for surface functionalization and nanoparticle deposition on the glass substrate.

2.2. Synthesis of gold nanoparticles (AuNPs)

Gold nanoparticles (AuNPs) were selected for this study because of their strong plasmonic response and proven suitability for ammonia detection [38]. The gold nanoparticles stabilized with citrate were synthesized following a modified Turkevich's method [39]. First, 80 μL of 50 mM aqueous gold (III) chloride solution was added to 19.92 mL of deionized (DI) water with continuous magnetic stirring. The mixture was heated to 70 °C at 600 rpm. Subsequently, 0.72 mL of 38.8 mM trisodium citrate (TSC) solution in DI water was added dropwise while stirring until the solution turned red, indicating successful formation of AuNPs. In this process, trisodium citrate (TSC) acts both as a reducing agent, converting Au^{3+} ions to metallic Au^0, and as a capping agent, providing negatively charged citrate groups on the nanoparticle surface. These surface charges create electrostatic repulsion, which helps stabilize the AuNPs and prevents aggregation. After completion, the mixture was rapidly cooled to 4 °C to stabilize the nanoparticles and prevent aggregation. The synthesis of citrated-stabilized AuNPs is shown in Fig. 1.

2.3. Fabrication of AuNP/PDDA layer on glass optical fiber

Following the synthesis of citrate-stabilized AuNPs, the next step was to immobilize them onto glass fiber substrates. For sensing applications, the AuNPs must be stabilized with homogeneous distribution and uniform surface coverage to maintain their optical response and avoid aggregation. Several methods exist for immobilizing AuNPs on glass surfaces, including solvent-evaporation assembly [40] and self-assembled monolayers [41], and polydopamine coatings [42]. Solvent evaporation often leads to aggregation, SAMs require multiple preparation steps, and polydopamine introduces additional optical absorption. In this work, PDDA-mediated electrostatic assembly offers a simple aqueous process that provides uniform coverage on cylindrical fibers with controllable AuNP density. These advantages support the use of the PDDA-based approach in this work.

Surface functionalized glass optical fibers with a cationic polyelectrolyte such as poly(diallydimethylammonium chloride) (PDDA) allow efficient deposition of negatively charged citrate-stabilized AuNPs [43–45]. The PDDA layers form a thin, uniform layer of positively

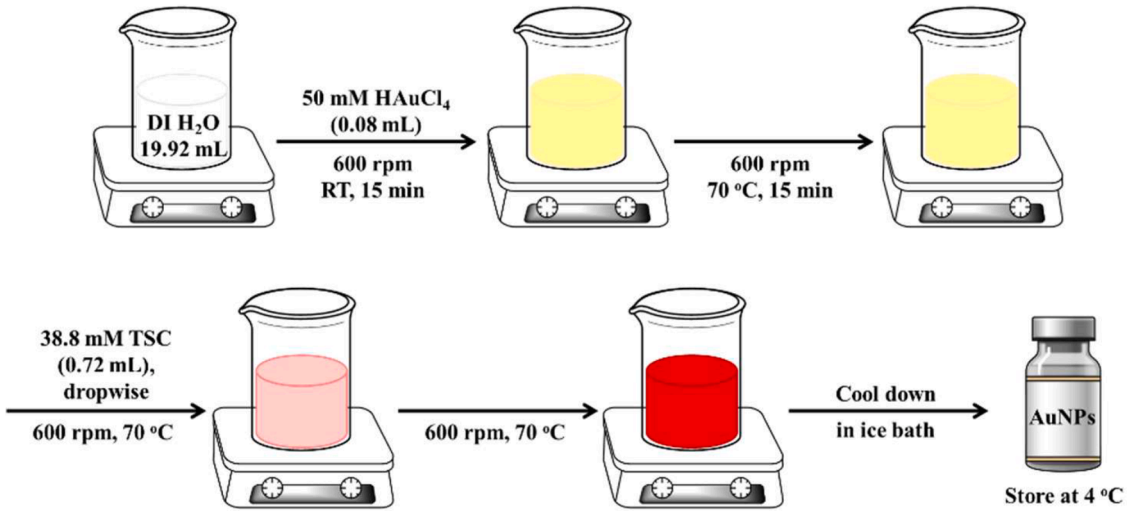

Fig. 1. Schematic of the synthesis of citrated-stabilized gold nanoparticles (AuNPs).

charged groups on the substrate, which serves as an electrostatically attractive anchoring matrix for the subsequent deposition of negatively charged particles. The resulting nanocomposite is therefore a promising engineered material for advanced applications, especially the detection of VOCs [15,46]. In this work, the positively charged PDDA layer provides cationic sites that electrostatically attract and attach the negatively charged citrate-stabilized AuNPs, enabling uniform immobilization on the substrate surface and resulting in a stable interface for sensing applications.

In fabricating AuNP/PDDA-functionalized layer on glass substrates, several parameters can significantly affect the quality and performance of the resulting films. Among these, the PDDA molecular weight, PDDA concentration, and AuNP deposition time are critical parameters that determine polymer chain conformation, surface coverage, functional group density, and the extent and uniformity of nanoparticle loading. These factors were therefore systematically investigated, as their optimization is essential to obtain stable interfacial properties and reproducible responses required for reliable sensing applications.

For the preparation of AuNP/PDDA-functionalized layer, the borosilicate glass substrates were ultrasonically cleaned in 1 M potassium hydroxide (KOH) solution for 10 min, then rinsed with DI water and isopropanol. The KOH treatment activates the glass surface by generating hydroxyl (-OH) groups, which serve as reactive sites for subsequent functionalization. This surface modification, known as silanization, facilitates the attachment of organosilane molecules [47]. Subsequently, the clean glass substrates were functionalized by immersion in a 4 % (v/v) APTES solution in ethanol at 60 °C for 1 h. Through this process, the surface -OH groups react with APTES to introduce amine (-NH_2) groups, providing functional sites for further immobilization [48]. After completion, the functionalized glass substrate were rinsed thoroughly with DI water. The APTES-functionalized substrates were then coated with low-MW PDDA at varying concentrations (0.05, 0.10, and 1 wt%) for 10 min, followed by rinsing with DI water to remove loosely bound polymer. Subsequently, the PDDA-coated glass substrates were immersed in the AuNPs colloidal solution for deposition times of 5, 10, 15, and 20 min to achieve uniform nanoparticle distribution. Following AuNP deposition, the substrates were rinsed with DI water to remove unbonded nanoparticles and dried at room temperature for 6 h. The same process was applied using medium-MW PDDA to evaluate the influence of molecular weight and concentration on sensor performance.

After establishing the fabrication process on borosilicate glass substrates, the method was applied to glass optical fibers to demonstrate their potential for sensing applications. The fabrication process of AuNPs immobilized on PDDA-coated glass optical fiber is shown in Fig. 2.

The fabrication process started with cleaning a 3.6 cm long NCF by sequential treatment with KOH, deionized water, and isopropanol, followed by functionalization with APTES. The APTES-functionalized optical fiber was then dip-coated in a solution of 1 wt% medium-MW PDDA and the gold colloidal solution for 10 and 20 min, respectively. This process was performed using a dip coating machine (Biolin Scientific, KSV NIMA, Sweden) at a 100 mm min^{-1} speed for 15 s. Accordingly, the dip-coating method was employed because it is a low-cost, solution-based method that affords conformal coverage on glass substrates and enables predictable thickness control through withdrawal speed and fluid properties, allowing for uniform nanometric coatings at room temperature [49]. After coating with PDDA and AuNPs, the fiber was dried at room temperature for 24 h. Finally, the AuNP/PDDA-coated fiber was spliced with single-mode fiber (SMF) at both ends using the splicer machine (Sumitomo Electric, Z2C, Japan). This application of optimized conditions in the fabrication of the optical fiber sensor was intended to maximize sensitivity for ammonia gas detection.

2.4. Preparation of ammonia gas (NH_3) concentrations and sensing setup

The AuNP/PDDA layer developed in this work represents a practical and novel material platform, and this study focuses on evaluating the influence of key fabrication parameters, including PDDA molecular weight, PDDA concentration, and AuNP deposition time. This systematic investigation highlights how these parameters affect material characteristics and performance, underscoring the versatility of the platform for a range of sensing applications. In this study, its applicability is demonstrated through ammonia (NH_3) detection, a target of interest for monitoring food spoilage.

To evaluate the NH_3 interaction with the AuNP/PDDA-coated optical fiber sensor, measurements were performed using gas concentrations ranging from 0.5 to 25 ppm. The lower concentrations (0.5–10 ppm) represent the range commonly associated with early-stage food spoilage, where ammonia serves as an indicator of protein degradation. The higher concentrations (15–25 ppm) correspond to the recommended occupational exposure limit for an 8 h working period [50]. This expanded range allows the sensor performance to be evaluated across both low- and high-level ammonia environments relevant to practical applications. Each NH_3 gas concentration was prepared in Tedlar bags, by using the ideal gas law (Eq. (1)) to find moles of NH_3 (n_{NH_3}):

$$n_{NH_3} = \frac{C_{ppm}}{10^6} \cdot n_{tot} \quad (1)$$

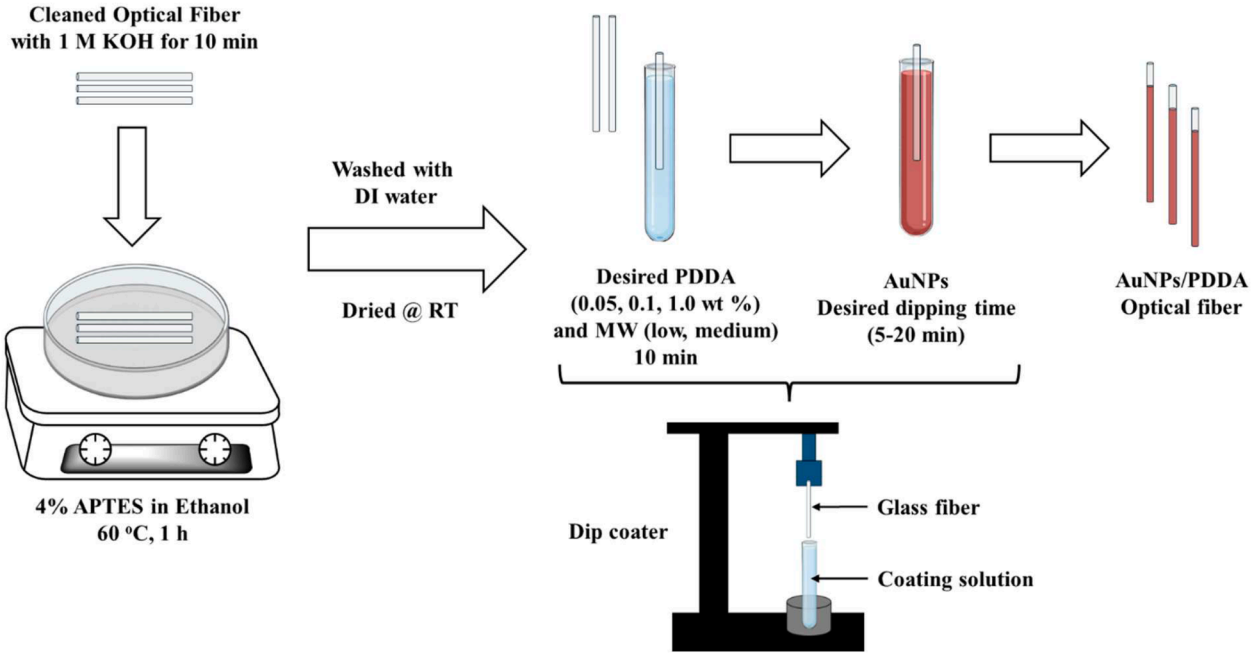

Fig. 2. Schematic of the fabrication process for depositing AuNPs onto PDDA-coated glass optical fibers.

where C_{ppm} represents thetargeted NH_3 gas concentration in ppm, $n_{tot} = \frac{PV}{RT}$ denotes the total moles of gas in the Tedlar bag, $P = 1$ atm (standard), $V = 1$ L (Tedlar bag volume), $R = 0.0821$ L•atm•mol^{-1}•K^{-1}, and $T = 298$ K. The required volume of NH_3 solution to be introduced into the Tedlar bag was then calculated using Eq. (2):

$$V_{NH_3} = \frac{n_{NH_3} \cdot M_{NH_3}}{\rho} \cdot \frac{1}{C_{NH_3}} \quad (2)$$

where $M_{NH_3} = 17.03$ g mol^{-1}, density (ρ) = 0.88 g mL^{-1}, and C_{NH_3} refers to the liquid NH_3 stock solution (30 wt%).

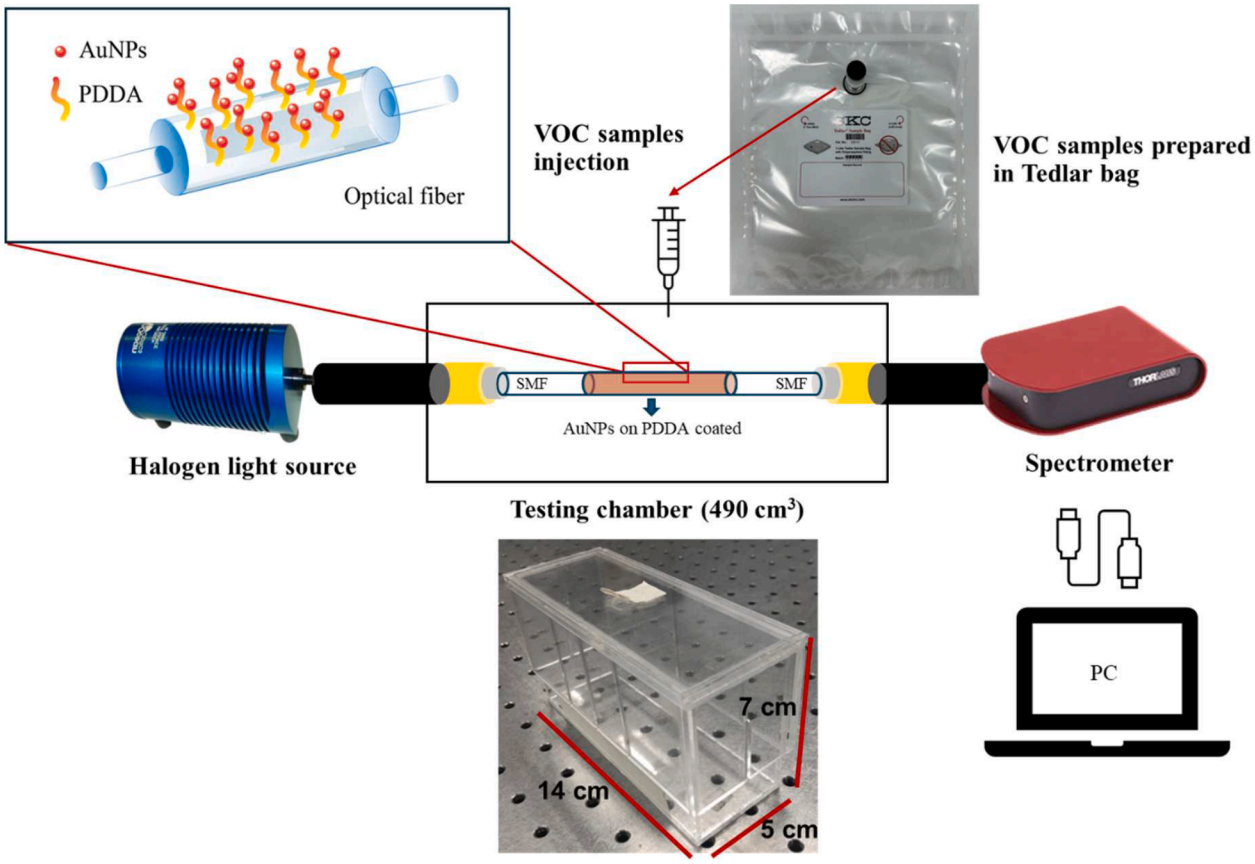

Fig. 3. Scheme diagram of AuNP/PDDA-functionalized optical fiber with VOC sensing setup.

To evaluate the sensing capability, the AuNP/PDDA-coated optical fiber was exposed to different ammonia concentrations inside the chamber using the optical measurement setup. The transmittance spectra and resonance wavelength shifts were monitored as the sensor responded to varying NH_3 levels. The optical testing configuration is illustrated in Fig. 3.

The calculated NH_3 gas was extracted and directly injected into a sealed chamber (490 cm^3) through the gas inlet. Prior to and after each exposure, nitrogen gas was used to purge residual gases to ensure measurement accuracy. The AuNP/PDDA-functionalized optical fiber sensor was placed inside the chamber and connected to a light source (Ocean Optics, HL-2000, USA), operating in the range 200–1100 nm, and to a spectrometer (Thorlabs, CCS200/M, USA). Optical signal from the light source were coupled to the sensor for wavelength shift measurements. Each experiment was repeated three times under controlled conditions, including atmospheric pressure, room temperature (25 °C), and 65 % relative humidity.

3. Results and discussion

3.1. Optical properties of AuNPs immobilized on PDDA layer

To verify the successful synthesis of AuNPs and their plasmonic response, the optical properties were investigated. The optical properties of the gold colloidal solution synthesized via the modified Turkevich's method were characterized using UV-Vis spectrometer (PerkinElmer, LAMBDA 850+, Waltham, MA, USA) in the 400–700 nm wavelength range, as shown in Fig. 4(a). The absorption spectrum exhibited a peak at 521 nm with a maximum absorbance of 0.9, which corresponds to the characteristic localized surface plasmon resonance (LSPR) of AuNPs in DI water at 525 nm, and is associated with average particle size in the range of 15–25 nm [51]. This result is consistent with the particle size averaging 22 nm obtained from dynamic light scattering (DLS) as shown in Fig. 4(b).

To enable stable and uniform AuNPs immobilization for sensing applications based on the LSPR mechanism, PDDA-assisted deposition was employed. The PDDA layer provides a positively charged surface that facilitates electrostatic attachment of the negatively charged citrate-stabilized AuNPs, thereby enhancing nanoparticle stability and distribution. To evaluate its effect on the optical response, AuNPs immobilized on a 1 wt% medium-MW PDDA-coated glass substrate were compared with AuNPs dispersed in deionized water. To assess the influence of PDDA-assisted deposition on the optical response, the absorption spectrum of AuNPs immobilized on a 1 wt% medium-MW PDDA-coated glass substrate was compared with that of AuNPs dispersed in DI water. The LSPR peak of AuNPs immobilized on the PDDA-coated glass substrate showed a redshift to 534 nm as illustrated in Fig. 4(a). The spectral shift is attributed to the increased refractive index surrounding the AuNPs, as they are electrostatically attached to the PDDA layer upon immobilization. This higher dielectric environment shifts the resonance to a longer wavelength.

3.2. Effect of PDDA molecular weight, concentration, and deposition time on AuNP immobilization

After establishing that AuNPs immobilized on PDDA-coated glass substrates exhibit a redshift in the LSPR peak, the effects of PDDA molecular weight, PDDA concentration, and AuNP deposition time on the optical properties were systematically investigated. These parameters dictate the density of cationic binding sites, the strength of electrostatic interactions with citrate-stabilized AuNPs, and the extent of nanoparticle attachment, thereby influencing nanoparticle density and distribution. Their evaluation is essential for establishing conditions that enable stable immobilization and reproducible optical responses for sensing applications. In this study, low- and medium-MW PDDA at concentrations of 0.05, 0.10, and 1 wt% were investigated, together with AuNP deposition times of 5, 10, 15, and 20 min. The LSPR absorption spectra for low-MW PDDA and medium-MW PDDA Fig. 5 and Fig. 6, respectively.

When comparing molecular weights, both low- and medium-MW PDDA produced similar linear growth trends. However, medium-MW PDDA yielded slightly higher absorbance under the same conditions. This difference is attributed to the greater chain length and flexibility of the medium-MW polymer, which allows chain looping and multiple interaction points, thereby allowing more AuNP attachment. On the other hand, low-MW PDDA forms shorter chains that adsorb more uniformly on the substrate, producing a consistent distribution of cationic sites but limiting the number of available binding sites. As a result, low-MW PDDA (Fig. 5) exhibited a stable baseline across concentrations with minimal drift, indicating high reproducibility. Medium-MW PDDA (Fig. 6), showed a concentration-dependent increase in absorbance, reflecting tunable adsorption behavior that enhances sensitivity.

The effect of PDDA concentration on AuNP immobilization is clearly observed in both low-MW (Fig. 5(a)–(c)) and medium-MW (Fig. 6(a)–(c)) systems. Higher PDDA concentrations at 1 wt%, produced stronger absorbance values at 534 nm compared with 0.10 and 0.05 wt%. This behavior reflects the greater density of cationic binding sites at higher concentrations, which enhances electrostatic attraction with the negatively charged citrate-stabilized AuNPs. Therefore, increasing PDDA concentration leads to improved nanoparticle immobilization, yielding

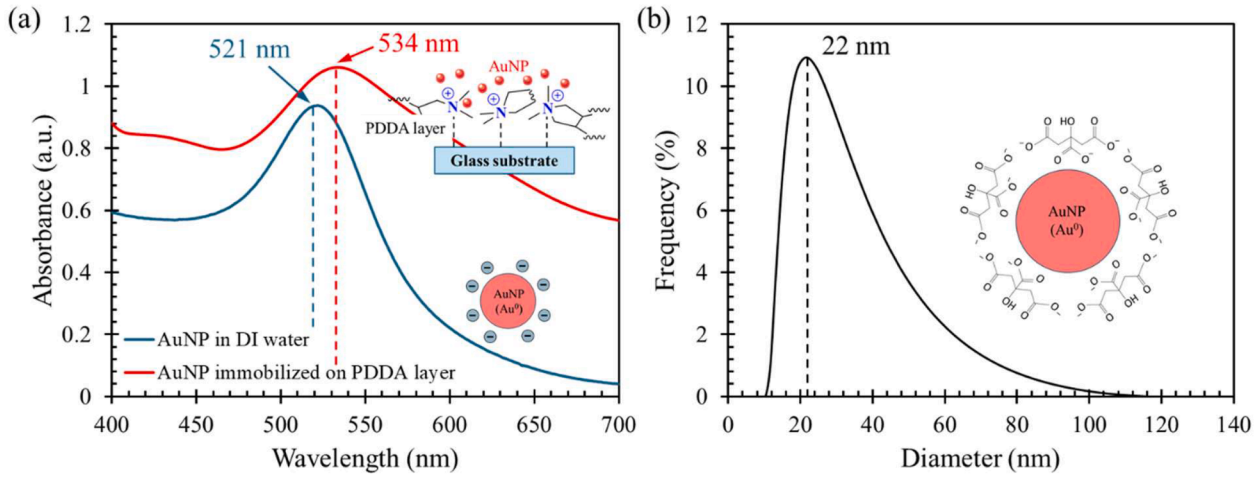

Fig. 4. (a) UV-Vis absorption spectra of colloidal AuNPs in DI water (blue) and AuNPs deposited on medium-MW PDDA (1 wt%) thin film coated on glass substrate (red). (b) Particle size distribution of colloidal AuNPs solution in DI water.

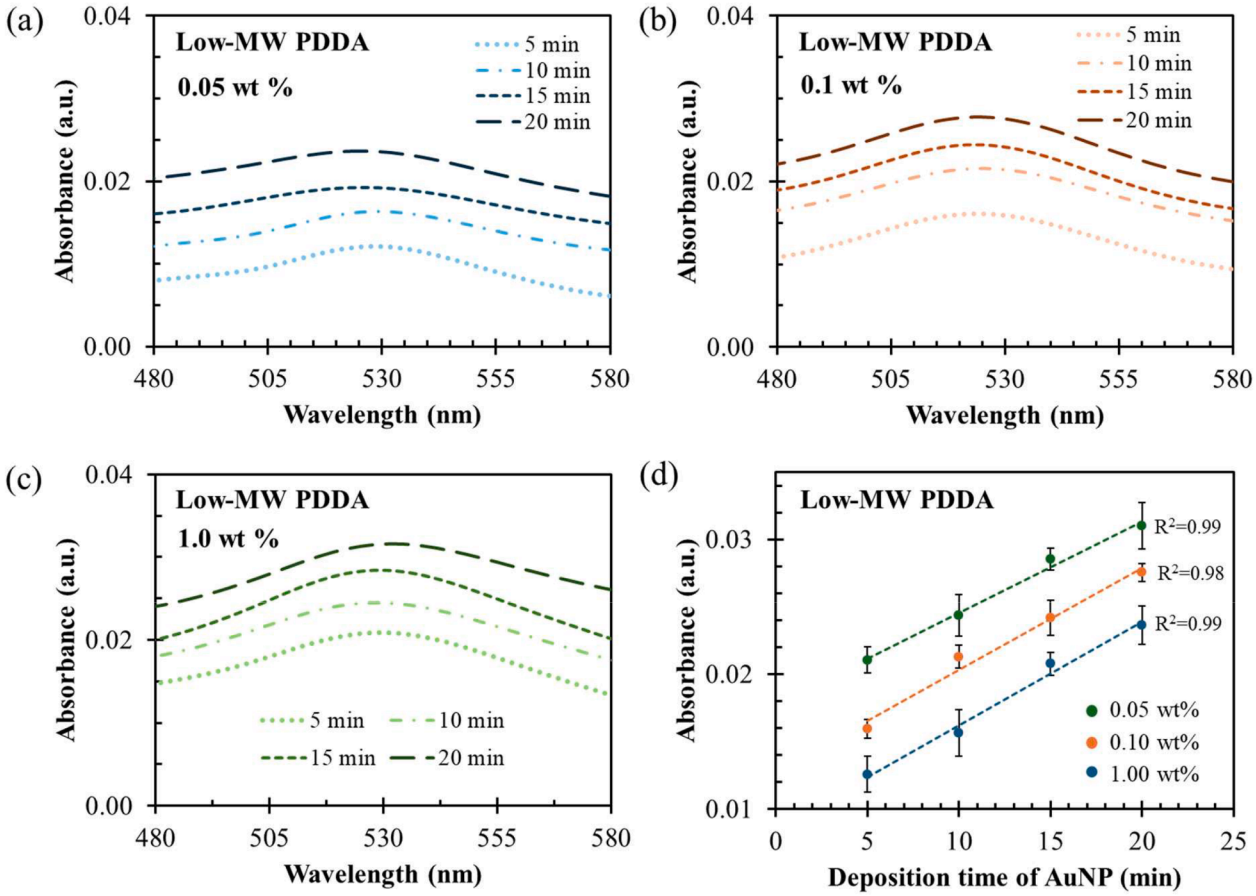

Fig. 5. LSPR absorption spectra of AuNPs deposited on glass substrates functionalized with low-MW PDDA at concentrations of (a) 0.05 wt%, (b) 0.10 wt%, and (c) 1 wt%. (d) Correlation between the average LSPR absorption peak and the AuNP deposition time for all three low-MW PDDA concentrations.

higher nanoparticle density, and a stronger LSPR signal.

Deposition time also plays a critical role in AuNP accumulation on the PDDA-coated substrates. Across all concentrations and molecular weights, absorbance increased linearly with gold deposition time in the range of 5–20 min, with strong correlations ($R^2 = 0.95$–0.99). This trend indicates that longer deposition times allow for progressive attachment of AuNPs to the polymer surface, leading to a more pronounced LSPR response. The linear dependence suggests that deposition kinetics under these conditions are well controlled, enabling predictable tuning of optical properties by varying deposition time.

Based on these results, 1 wt% medium-MW PDDA with a 20 min AuNP deposition time was selected as the optimal condition for fabricating the AuNP/PDDA-coated optical fiber sensor, which was subsequently tested for NH_3 detection in this paper for potential application.

3.3. Surface morphology and coverage of AuNP/PDDA layers

To investigate the effect of PDDA molecular weight, concentration, and AuNP deposition time on nanoparticle immobilization, the surface morphology of the AuNPs immobilized on PDDA-coated glass substrate was examined using atomic force microscopy (AFM) and field-emission scanning electron microscopy (FE-SEM). The analysis aimed to establish a quantitative relationship between these parameters and AuNP adsorption behavior, including surface coverage, and distribution.

3.3.1. Atomic force microscopy (AFM)

AFM was used to evaluate the average surface roughness (R_a) of the AuNP/PDDA-coated glass substrates. Surface roughness provides a quantitative measure of nanoscale topography that reflects nanoparticle immobilization. Higher R_a values correspond to denser nanoparticle coverage, whereas lower R_a values indicate smoother surfaces with reduced coverage. Comparing R_a across different PDDA molecular weights, concentrations, and AuNP deposition times allows the relationship between polymer parameters and nanoparticle assembly to be determined, which is critical for further sensing applications. The R_a values of AuNPs deposited on PDDA-coated glass substrates are summarized in Table 1.

A clear dependence of R_a on deposition time is observed. At short AuNP deposition times (5–10 min), the R_a values remain relatively low, reflecting partial nanoparticle coverage with dispersed AuNPs. As deposition time increases to 15–20 min, R_a values increase, reaching up to 7.4 nm, which indicates denser nanoparticle attachment. These results confirm that deposition time plays a critical role for the nanoparticle accumulation.

The effect of PDDA concentration is also evident across all AuNP deposition times. Higher concentrations result in increased R_a values by providing additional cationic binding sites for electrostatic interactions with negatively charged citrate-stabilized AuNPs. This trend demonstrates that higher PDDA concentrations lead to denser nanoparticle immobilization and increased rougher surfaces.

A comparison between low- and medium-MW PDDA reveals that differences in R_a are less significant at short deposition times (5–10 min) but become more pronounced with longer deposition. At 20 min and 1 wt% PDDA, R_a reaches 6.3 ± 1.1 nm for low-MW PDDA and 7.4 ± 1.4 nm for medium-MW PDDA. This result indicates that the longer, more flexible chains of medium-MW PDDA promote greater nanoparticle accumulation over time compared with the shorter chains of low-MW PDDA. These observations are consistent with the absorption spectra shown in Figs. 5 and 6 with previous studies reporting increased roughness in polyelectrolyte-nanoparticle systems with extended chain

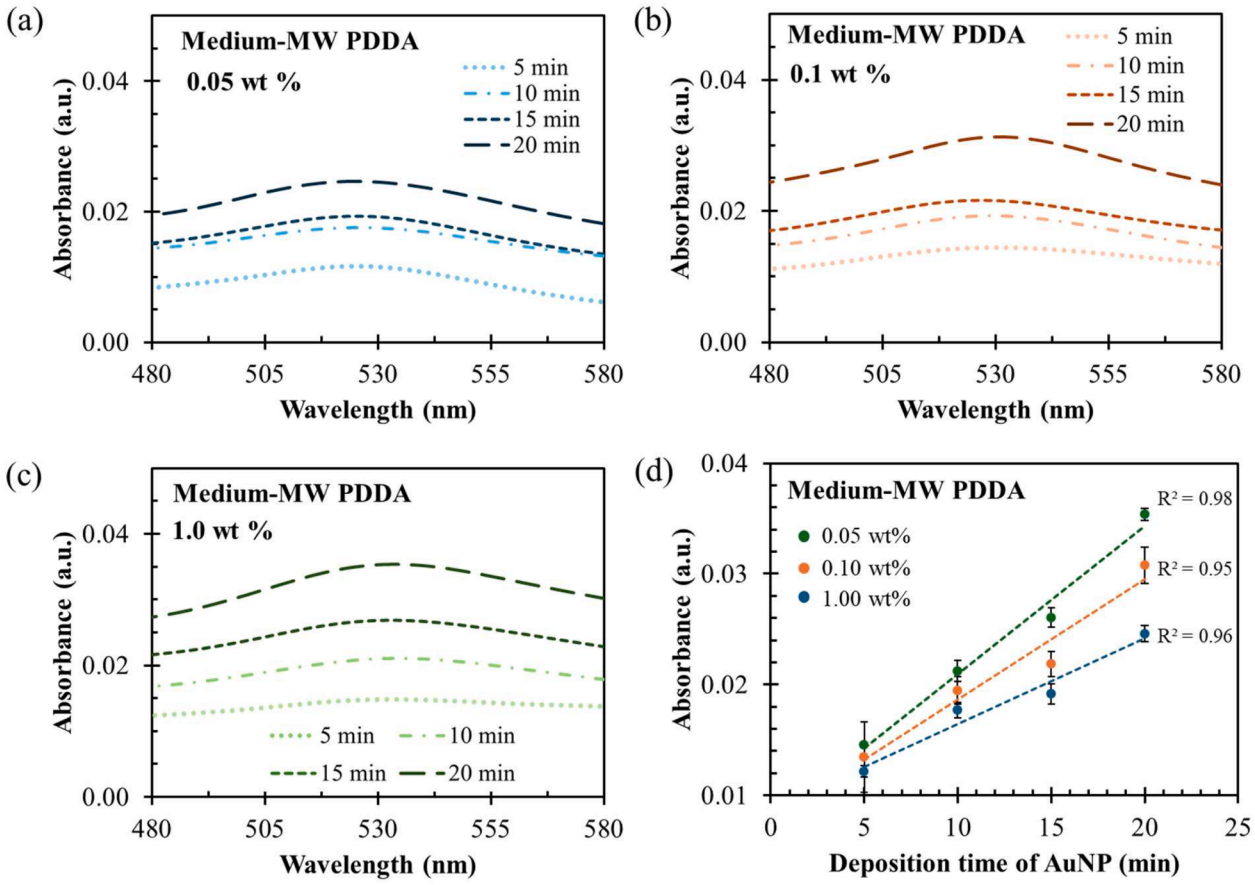

Fig. 6. LSPR absorption spectra of AuNPs deposited on glass substrates functionalized with medium-MW PDDA at concentrations of (a) 0.05 wt%, (b) 0.10 wt%, and (c) 1 wt%. (d) Correlation between the average LSPR absorption peak and the AuNP deposition time for all three medium-MW PDDA concentrations.

Table 1
Average surface roughness (R_a) of AuNPs deposited on PDDA-coated glass substrates with varying PDDA molecular weight, concentration, and AuNP deposition time.

AuNP deposition time (min)	MW	Average Roughness, R_a (nm)		
		0.05 wt%	0.10 wt%	1 wt%
5	Low	1.1 ± 0.2	3.0 ± 0.5	3.2 ± 0.4
	Medium	1.0 ± 0.2	2.7 ± 0.4	3.3 ± 0.4
10	Low	2.0 ± 0.3	3.8 ± 0.5	3.7 ± 0.5
	Medium	2.6 ± 0.1	3.3 ± 0.3	4.0 ± 0.4
15	Low	3.6 ± 0.2	4.0 ± 0.4	4.1 ± 0.4
	Medium	4.6 ± 0.8	5.7 ± 0.8	6.3 ± 0.6
20	Low	5.0 ± 0.9	6.0 ± 0.6	6.3 ± 1.1
	Medium	5.1 ± 0.4	6.3 ± 0.8	7.4 ± 1.4

architecture [52,53].

3.3.2. *Field-emission scanning electron microscopy (FE-SEM)*

FE-SEM was used to visualize the surface morphology of the AuNP/PDDA-coated glass optical fiber. It provides direct imaging of nanoparticle attachment and distribution over larger surface areas. SEM images allow the identification of particle aggregation, surface uniformity, and coverage density, thereby complementing AFM measurements. By comparing SEM images across different PDDA molecular weights, concentrations, and deposition times, qualitative confirmation of nanoparticle attachment and distribution can be obtained, supporting the quantitative roughness analysis. To assess the effect of deposition time on AuNP immobilization, FE-SEM imaging was performed on glass optical fibers coated with low- and medium-MW PDDA at a fixed concentration of 1 wt%, as shown in Fig. 7.

It can be seen from the FE-SEM images that deposition time and PDDA molecular weight strongly influence AuNP immobilization on the glass optical fiber surface. At 5 min (Fig. 7(a)), both low- and medium-MW PDDA show limited nanoparticle attachment, although medium-MW PDDA exhibits slightly higher particle density. At 10 min Fig. 7 (b)), nanoparticle coverage increases significantly for both systems. At 15 min (Fig. 7(c)), extensive coverage is observed, with medium-MW PDDA maintaining a higher density. By 20 min (Fig. 7(d)), near-saturation coverage is achieved, with medium-MW PDDA supporting slightly greater immobilization than low-MW PDDA.

The quantitative analysis of surface particle-covered density (% AuNPs) presented in Fig. 7(e)) confirms these observations. The analysis was carried out by image-based evaluation of SEM micrographs, allowing estimation of the percentage of surface area covered by nanoparticles. Particle coverage steadily increases with deposition time, from 1.95 % (low-MW) and 3.03 % (medium-MW) at 5 min to 16.7 % and 18.5 %, respectively, at 20 min. Medium-MW PDDA consistently yields higher coverage across all deposition times, reflecting its ability to promote more efficient nanoparticle attachment.

For the lower range (5–10 min), it clearly shows limited surface coverage with large interparticle gaps, as observed from FE-SEM images. With increasing deposition time, coverage increases and approaches saturation. Between 10 and 20 min, the change in surface-covered area is <0.4 %, indicating that the immobilization process is approaching its effective maximum loading on the PDDA layer. Extending deposition time beyond this point would further narrow interparticle spacing and increase particle–particle contact, promoting clustering and reducing uniformity. Therefore, we select 20 min as the condition that maximizes the signal while keeping aggregation low.

Uniformity was also evaluated by analyzing the surface-covered

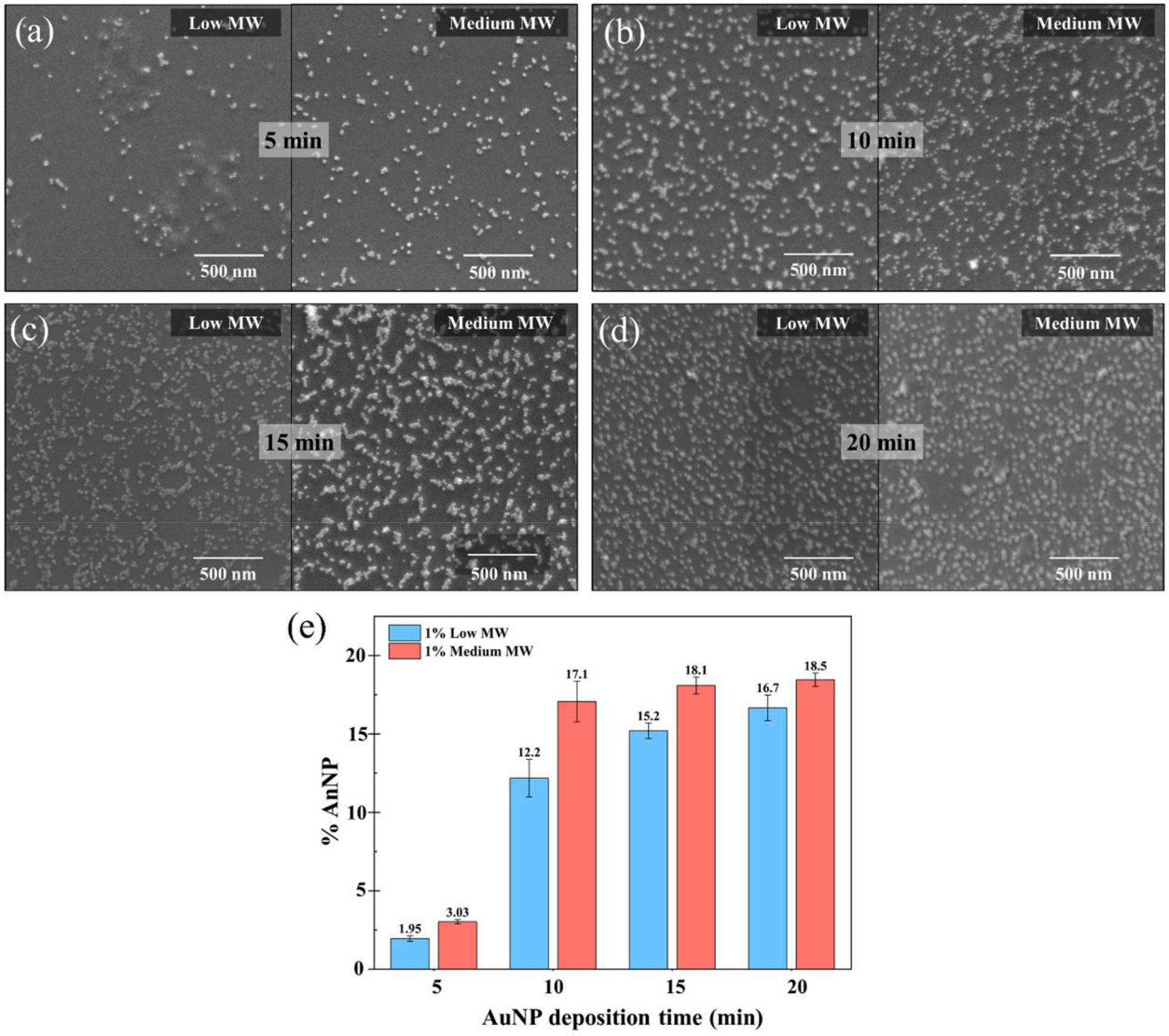

Fig. 7. FE-SEM images of AuNPs deposited on glass optical fiber coated with low- and medium-MW PDDA at a fixed concentration of 1 wt% with deposition times of (a) 5 min, (b) 10 min, (c) 15 min, and (d) 20 min. (e) Quantitative analysis of surface particle-covered density (% AuNPs).

fraction across multiple regions of the SEM image. The mean coverage of 18.1 % ± 0.27 % and a coefficient of variation (CV) of 1.49 % confirm that the AuNPs are uniformly distributed on 1 % medium-MW PDDA, with only minor clustering that does not affect the continuity of the plasmonic layer.

These results are consistent with AFM roughness data (Table 1) and UV–Vis absorption spectra (Figs. 5 and 6), demonstrating that increased surface coverage directly enhances the LSPR response.

3.4. Verification of NH_3 adsorption at the AuNP/PDDA interface

The next study focused on confirming whether the fabricated AuNP/PDDA-coated glass substrate could detect the presence of NH_3. The glass substrates were prepared under the optimized conditions of 1 wt% medium-MW PDDA and 20 min AuNP deposition, and subsequently exposed to NH_3. Fourier-transform infrared (FTIR) spectroscopy was used to monitor the chemical interaction between the AuNP/PDDA coating layer and NH_3 molecules. This test provides direct spectroscopic evidence of adsorption and validates the suitability of the functionalized substrate for subsequent sensing experiments. The AuNP/PDDA-coated glass substrate was exposed to 10 and 20 ppm NH_3 in a closed chamber for 12 min at room temperature and 65 % relative humidity. FTIR spectroscopy was then employed to investigate the chemical interactions between NH_3 molecules and the functional groups within the AuNP/PDDA layer. The FTIR results are presented in Fig. 8.

There are distinct spectral changes in two key regions, including the broad N-H stretching band at 3400–3150 cm^{-1} and the discrete N-H bending mode at 1545 cm^{-1}. In the absence of NH_3, both features are weak, reflecting the quaternary ammonium structure of PDDA with limited available N-H groups. Upon NH_3 exposure, the stretching band broadens and increases in intensity, while the bending mode becomes more pronounced and grows with increasing concentration. The increase in intensity of the 1545 cm^{-1} bending band with NH_3 demonstrates its potential as a quantitative indicator, while the 3400–3150 cm^{-1} stretching feature serves as a complementary qualitative marker for NH_3 detection under ambient conditions [50]. These spectral variations confirm the successful adsorption of NH_3 molecules onto the AuNP/PDDA-coated layer, indicating effective chemical interaction at the interface. The observed adsorption behavior supports the suitability of this material system for ammonia sensing applications.

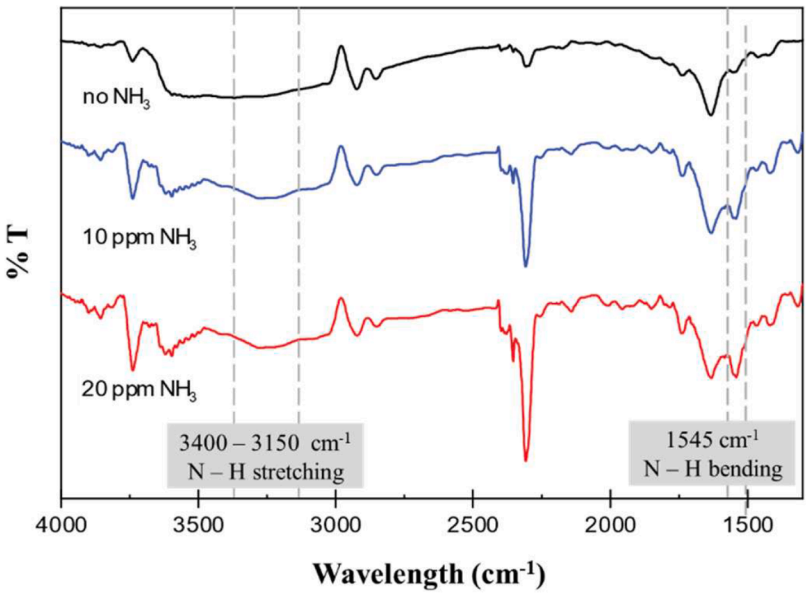

Fig. 8. FTIR spectra of AuNP/PDDA-coated glass substrates exposed to NH_3 gas at 0, 10 and 20 ppm.

3.5. Ammonia detection performance of the AuNP/PDDA-coated optical fiber

From the combined optical, morphological, and surface roughness analyses, the optimal condition for sensing application was identified as 1 wt% medium-MW PDDA with a 20 min AuNP deposition time. Under this condition, the AuNP/PDDA-coated optical fiber exhibits enhanced nanoparticle coverage, stable immobilization, and a strong LSPR response, making it suitable for gas detection. Based on these findings, the sensor was further evaluated by exposing it to different concentrations of NH_3 to investigate its detection capability.

3.5.1. Sensing mechanism

The preparation of the AuNP/PDDA-functionalized layer on the glass optical fiber is crucial for achieving reliable sensing performance. The glass surface is first thoroughly cleaned, and KOH treatment activates the surface by generating hydroxyl (-OH) groups, which serve as reactive sites for subsequent functionalization. These surface -OH groups react with APTES to introduce amine (-NH_2) groups, enabling the electrostatic adsorption of a thin PDDA layer by dip-coating. The cationic PDDA then captures citrate-stabilized AuNPs, yielding a conformal nanoparticle layer. This sequential process produces a thin interface on glass fiber that is well-suited for sensing of NH_3 via wavelength interrogation.

The sensing mechanism of the AuNP/PDDA-coated optical fiber is primarily attributed to electrostatic interactions between the negatively charged citrate-stabilized gold nanoparticles and the partially positively charged protons of NH_3 molecules as shown in Fig. 9. Adsorption of NH_3 onto the AuNP surface perturbs the local dielectric environment and alters the LSPR, producing a measurable optical response. With the change in NH_3 concentration, the amount of molecular adsorption on the optical fiber surface changes, leading to a wavelength shift in the transmittance spectra. This mechanism provides an effective transduction pathway, enabling reliable and sensitive detection of ammonia.

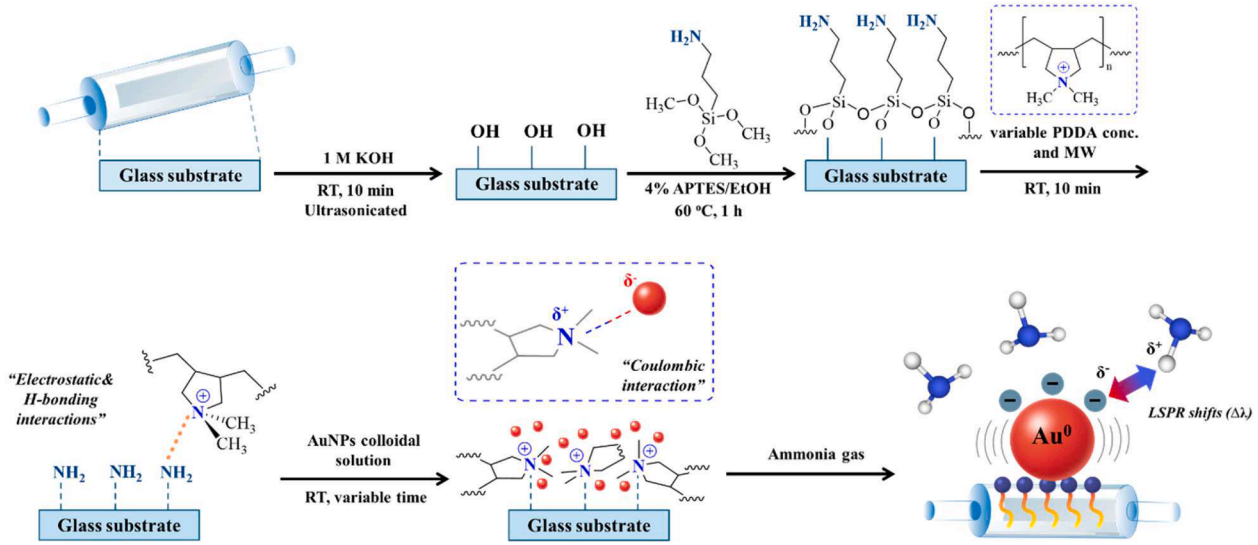

Fig. 9. Schematic illustration of the NH_3 sensing mechanism on the AuNP/PDDA-functionalized optical fiber, showing surface functionalization, AuNP immobilization, and ammonia adsorption at the plasmonic interface.

3.5.2. Transmittance spectra and resonance wavelength shift

The transmittance spectra (T) of the AuNP/PDDA-coated optical fiber were measured under different NH_3 concentration of 0.5, 1, 5, 10, 15, 20, and 25 ppm. Air was used as the reference medium, and desorption of NH_3 was carried out using a nitrogen purge, ensuring reversibility of the sensing process and enabling repeated sensor use with stable performance. The resulting transmittance spectra are showing in Fig. 10(a). Transmittance was calculated according to Eq. (3)

$$T = \frac{I}{I_0} \tag{3}$$

where I is the transmitted light intensity through the sensor during NH_3 exposure, and I_0 is the transmitted intensity measured under the reference condition, which is air.

The AuNP/PDDA-coated fiber exhibits a resonance dip at ~616 nm due to the hybrid LSPR–waveguide interaction with the evanescent field. The guided mode senses the effective refractive index surrounding the fiber rather than the intrinsic free-space plasmon resonance, leading to a redshift and a different spectral position of the resonance feature compared with the ~530 nm peak measured in free-space. With increasing NH_3 concentration, the extent of adsorption correspondingly increases, leading to a progressive redshift in the resonance wavelength.

3.5.3. Sensitivity and repeatability

The sensor response can be quantitatively expressed in terms of sensitivity (S), defined as the change in resonance wavelength relative to the change in NH_3 concentration (Eq. (4)).

$$S = \frac{\Delta wavelength}{\Delta concentration} \tag{4}$$

Measurements were performed at room temperature and 65 % relative humidity. A strong linear correlation was obtained with a regression coefficient of 0.99, confirming the reliability of the response and the stability of the AuNP/PDDA interface, as shown in Fig. 10(b). Under these conditions, the sensor demonstrated a sensitivity of 0.023 nm/ppm, highlighting its capability for ammonia detection.

The sensing measurements were repeated three times under identical conditions to assess repeatability. The error bars shown in Fig. 10(b) represent the standard deviation of replicate measurements at each NH_3 concentration. The small deviations indicate good measurement consistency, confirming that the AuNP/PDDA-functionalized optical fiber provides reliable and reproducible spectral responses across multiple sensing cycles.

3.5.4. Performance comparison with existing NH_3 sensor

The performance comparison between AuNP/PDDA-coated optical fiber and previously reported sensors are summarized in Table 2. The developed sensor in this work offers a competitive combination of sensitivity and low-ppm detection under simple fabrication conditions. Inorganic and hybrid systems, such as GO-ZnO nanocomposites and Au-coated ZnO nanostructures, exhibit higher reported sensitivities of 0.031 and 0.093 nm/ppm, respectively, but either require more complex nanostructure or operate over relatively narrow ranges [54,55]. Polymer-based coatings, including PAA/PANI and PDMS/PMMA composites, show lower sensitivities of 0.0098 and 0.00418 nm/ppm, respectively, although they can operate over broader ranges up to 50–200 ppm [56,57]. In addition, silica- and oxide-based films, such as GO (0.00497 nm/ppm), silica gel (0.0148 nm/ppm), and Fe_2O_3 nanotubes (0.0013 nm/ppm), show modest sensitivities despite their wider detection ranges extending up to 100–11,640 ppm [58–60]. The Au/PDDA coating in this work achieves a sensitivity of 0.023 nm/ppm over the 0–25 ppm NH_3 range, which is higher than that of most polymer and silica systems. This sensitivity is comparable in magnitude to PANI graphene structures [61].

Table 2
Comparison of ammonia sensing performance of various optical fiber–based sensing materials, including detection range and wavelength sensitivity.

Sensing materials	NH_3 detection range (ppm)	Sensitivity (nm/ppm)	Ref
Inorganic/oxide/hybrid			
GO-ZnO nanocomposite	4–140	0.031	[54]
Au-coated ZnO nanostructures	0–10	0.093	[55]
Fe_2O_3 nanotube	0–11,640	0.00130	[60]
Silica gel	0–100	0.0148	[59]
Carbon/polymer composite			
Graphene Oxide (GO)	0–151	0.00497	[58]
PANI-graphene	0–100	−0.0278	[61]
PAA/PANI	0–50	0.0098	[56]
PDMS/PMMA	0–200	0.00418	[57]
Polymer nanocomposite			
AuNP/PDDA	0–25	0.023	This work

In this work, the proposed AuNP/PDDA-functionalized optical fiber sensor demonstrates clear advantages in terms of simplicity, stability, and sensitivity. The incorporation of PDDA provides a robust matrix for stabilizing gold nanoparticles, ensuring uniform immobilization and preventing aggregation, while simultaneously contributing to molecular adsorption. This innovative configuration enables reliable ammonia detection under ambient conditions without complex instrumentation. The straightforward fabrication and reusability of the sensor highlight its potential for practical deployment in environmental, industrial, and healthcare monitoring.

The sensing results presented here serve as a proof of concept to

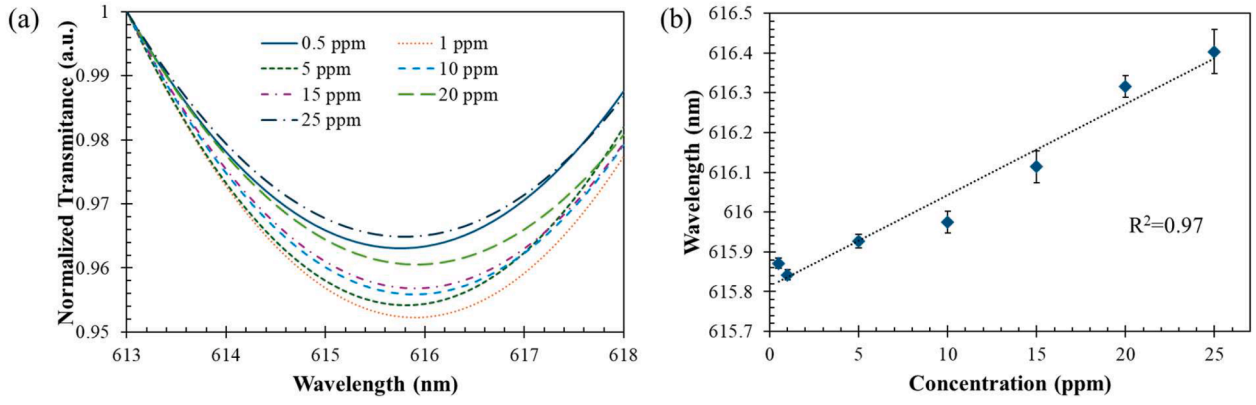

Fig. 10. (a) Transmittance spectra of AuNP/PDDA-coated optical fiber sensor under NH_3 exposure (0.5–25 ppm) at 616 nm operating wavelength. (b) Sensitivity response of the proposed fiber sensor, showing correlation between NH_3 concentration over wavelength shift.

demonstrate the integration of the optimized AuNP/PDDA interface onto an optical fiber as a potential application for sensing. Full sensor validation, including long-term stability, repeatability, and specificity, will be addressed in future work.

4. Conclusions

Gold nanoparticles (AuNPs) were immobilized on an optical fiber surface using poly(diallyldimethylammonium chloride) (PDDA) as a stabilizing and supporting matrix for ammonia sensing. To optimize the coating process, PDDA concentration, PDDA molecular weight, and AuNP deposition time were systematically varied. The optimum condition was identified as 1 wt% medium-molecular-weight PDDA with a 20 min AuNP deposition, which produced uniform nanoparticle coverage, stable immobilization, and a strong plasmonic response. Characterization by FE-SEM, AFM, and FTIR confirmed the homogeneous distribution of AuNPs, suitable surface roughness, and specific adsorption of NH_3 at the AuNP/PDDA interface. The AuNP/PDDA platform was applied on an optical fiber to evaluate its sensing capability with ammonia at concentrations of 0.5, 1, 5, 10, 15, 20, and 25 ppm under room temperature. The sensor exhibited clear concentration-dependent spectral shifts with a sensitivity of 0.023 nm/ppm and strong linearity ($R^2 = 0.97$). These results demonstrate that systematic material optimization yields a robust and stable sensing interface, highlighting improvement in interfacial stability and the potential of the AuNP/PDDA-functionalized optical fiber for practical ammonia monitoring in environmental, industrial, and healthcare applications.

Funding sources

This work was financially supported by Thailand Science research and Innovation Fund Chulalongkorn University (IND_FF_69_091_2100_014); the Secondary Century Fund (C2F); and the Rachadapisek Sompote Fund for Biomedical Materials and Devices for Revolutionary Integrative Systems Engineering Research Unit (BMD-RISE), Chulalongkorn University.

CRediT authorship contribution statement

Ratchawi Jammee: Writing – original draft, Validation, Methodology, Investigation, Formal analysis, Data curation. **Pannathorn Jitpratak:** Investigation, Formal analysis. **Abinash Panda:** Investigation, Data curation. **Paris Uerchuchai:** Investigation, Data curation. **Parinthorn Trakarnvanich:** Data curation. **Akhilesh Kumar Pathak:** Writing – review & editing, Conceptualization. **Charusluk Viphavakit:** Writing – review & editing, Supervision, Resources, Project administration, Methodology, Funding acquisition, Conceptualization.

Declaration of competing interest

The authors declare that they have no known competing financial interests or personal relationships that could have appeared to influence the work reported in this paper.

Data availability

Data will be made available on request.

References

[1] E. David, V.-C. Niculescu, Volatile organic compounds (VOCs) as environmental pollutants: occurrence and mitigation using nanomaterials, Int. J. Environ. Res. Public Health (2021) 18.
[2] S.H. Shin, W.K. Jo, Volatile organic compound concentrations, emission rates, and source apportionment in newly-built apartments at pre-occupancy stage, Chemosphere 89 (5) (2012) 569–578.
[3] J.A. Bernstein, et al., The health effects of nonindustrial indoor air pollution, J. Allergy Clin. Immunol. 121 (3) (2008) 585–591.
[4] J.M. Gostner, et al., Cellular reactions to long-term volatile organic compound (VOC) exposures, Sci. Rep. 6 (1) (2016) 37842.
[5] D. Kwak, Y. Lei, R. Maric, Ammonia gas sensors: a comprehensive review, Talanta 204 (2019) 713–730.
[6] Agency for Toxic Substances and Disease Registry (ATSDR) toxicological profiles, Toxicological Profile for Ammonia, Agency for Toxic Substances and Disease Registry (US), Atlanta (GA), 2004.
[7] H. Tai, et al., Enhanced ammonia response of Ti3C2Tx nanosheets supported by TiO2 nanoparticles at room temperature, Sens. Actuators B: Chem. 298 (2019) 126874.
[8] L.A. Panes-Ruiz, et al., Toward highly sensitive and energy efficient ammonia gas detection with modified single-walled carbon nanotubes at room temperature, ACS Sens. 3 (1) (2018) 79–86.
[9] C. Mackin, et al., Chemiresistive graphene sensors for ammonia detection, ACS Appl. Mater. Interfaces 10 (18) (2018) 16169–16176.
[10] X. Li, et al., WS2 nanoflakes based selective ammonia sensors at room temperature, Sens. Actuators B: Chem. 240 (2017) 273–277.
[11] Y. Wang, et al., NH3 gas sensing performance enhanced by Pt-loaded on mesoporous WO3, Sens. Actuators B: Chem. 238 (2017) 473–481.
[12] J. Johny, S. Amos, R. Prabhu, Optical fibre-based sensors for oil and gas applications, Sensors 21 (18) (2021) 6047.
[13] A. Leal-Junior, et al., The role of optical fiber sensors in the new generation of healthcare devices: a review, Sens. Diagn. 3 (7) (2024) 1135–1158.
[14] C. Love, et al., A review on advanced sensing materials for agricultural gas sensors, Sensors 21 (10) (2021) 3423.
[15] A.K. Pathak, C. Viphavakit, A review on all-optical fiber-based VOC sensors: heading towards the development of promising technology, Sens. Actuators A: Phys. 338 (2022) 113455.
[16] N. Sabri, S.A. Aljunid, M.S. Salim, S. Fouad, Fiber Optic Sensors: Short Review and Applications, Springer, Singapore, 2015, pp. 299–311.
[17] Y. Zhao, J. Zhao, Q. Zhao, Review of no-core optical fiber sensor and applications, Sens. Actuators A: Phys. 313 (2020) 112160.
[18] M.F. Bado, J.R. Casas, A review of recent distributed optical Fiber sensors applications for civil engineering structural health monitoring, Sensors 21 (5) (2021) 1818.
[19] J. Li, et al., Preparation and application of metal nanoparticals elaborated Fiber sensors, Sensors 20 (18) (2020) 5155.
[20] R.A. Minz, S.S. Pal, R.K. Sinha, S.K. Mondal, Plasmonic coating on chemically treated optical Fiber probe in the presence of evanescent wave: a novel approach for designing sensitive Plasmonic sensor, Plasmonics 11 (2) (2016) 653–658.
[21] A. Urrutia, J. Goicoechea, F.J. Arregui, Optical Fiber sensors based on nanoparticle-embedded coatings, J. Sens. 2015 (2015) 1–18.
[22] K. Saha, et al., Gold nanoparticles in chemical and biological sensing, Chem. Rev. 112 (5) (2012) 2739–2779.
[23] Y.-C. Yeh, B. Creran, V.M. Rotello, Gold nanoparticles: preparation, properties, and applications in bionanotechnology, Nanoscale 4 (6) (2012) 1871–1880.
[24] N. Elahi, M. Kamali, M.H. Baghersad, Recent biomedical applications of gold nanoparticles: a review, Talanta 184 (2018) 537–556.
[25] C.-C. Chang, et al., Gold nanoparticle-based colorimetric strategies for chemical and biological sensing applications, Nanomaterials 9 (6) (2019) 861.
[26] S. Palani, et al., Multispectral localized surface plasmon resonance (msLSPR) reveals and overcomes spectral and sensing heterogeneities of single gold nanoparticles, ACS Nano 17 (3) (2023) 2266–2278.
[27] J. Homola, S.S. Yee, G. Gauglitz, Surface plasmon resonance sensors: review, Sens. Actuators B: Chem. 54 (1) (1999) 3–15.
[28] K.A. Willets, R.P. Van Duyne, Localized surface plasmon resonance spectroscopy and sensing, Annu. Rev. Phys. Chem. 58 (2007) 267–297 (Volume 58, 2007).
[29] G. Li, et al., Slide-type waveflex biosensor based on signal enhancement technology for alpha-fetoprotein detection, Opt. Lett. 48 (18) (2023) 4745–4748.
[30] G. Li, et al., Nb2CTx MXene-assisted double S-tapered fiber-based LSPR sensor with improved features for tyramine detection, Appl. Phys. Lett. (8) (2023) 122.
[31] H.H. Kyaw, S.H. Al-Harthi, A. Sellai, J. Dutta, Self-organization of gold nanoparticles on silanated surfaces, Beilstein J. Nanotechnol. 6 (1) (2015) 2345–2353.
[32] M. Ben Haddada, et al., Optimizing the immobilization of gold nanoparticles on functionalized silicon surfaces: amine-vs thiol-terminated silane, Gold Bull. 46 (4) (2013) 335–341.
[33] Y. Niidome, et al., Immobilization of gold nanorods on the glass substrate by the electrostatic interactions for localized plasmon sensing, Chem. Lett. 33 (4) (2004) 454–455.
[34] Y. Chaikin, et al., Stabilization of metal nanoparticle films on glass surfaces using ultrathin silica coating, Anal. Chem. 85 (21) (2013) 10022–10027.
[35] I. Ruach-Nir, et al., Silica-stabilized gold island films for transmission localized surface plasmon sensing, J. Am. Chem. Soc. 129 (1) (2007) 84–92.
[36] C.J. Murphy, et al., Anisotropic metal nanoparticles: synthesis, assembly, and optical applications, J. Phys. Chem. B 109 (29) (2005) 13857–13870.
[37] W. Yim, et al., Gold nanorod–Melanin hybrids for enhanced and prolonged photoacoustic imaging in the near-infrared-II window, ACS Appl. Mater. Interfaces 13 (13) (2021) 14974–14984.
[38] H. Naderi, et al., Sensitive, selective and rapid ammonia-sensing by gold nanoparticle-sensitized V2O5/CuWO4 heterojunctions for exhaled breath analysis, Appl. Surf. Sci. 501 (2020) 144270.
[39] J. Kimling, et al., Turkevich method for gold nanoparticle synthesis revisited, J. Phys. Chem. B 110 (32) (2006) 15700–15707.

[40] T.K. Sau, C.J. Murphy, Self-assembly patterns formed upon solvent evaporation of aqueous cetyltrimethylammonium bromide-coated gold nanoparticles of various shapes, Langmuir 21 (7) (2005) 2923–2929.
[41] S.M. Marinakos, S. Chen, A. Chilkoti, Plasmonic detection of a model analyte in serum by a gold nanorod sensor, Anal. Chem. 79 (14) (2007) 5278–5283.
[42] P.J. Rivero, J. Goicoechea, F.J. Arregui, Layer-by-Layer nano-assembly: a powerful tool for optical Fiber sensing applications, Sensors 19 (3) (2019) 683.
[43] M.M. Ottakam Thotiyl, et al., Multilayer assemblies of polyelectrolyte–gold nanoparticles for the electrocatalytic oxidation and detection of arsenic(III), J. Colloid. Interface Sci. 383 (1) (2012) 130–139.
[44] Y. Guo, D. Wang, L. Yang, S. Liu, Nanoscale monolayer adsorption of polyelectrolytes at the solid/liquid interface observed by quartz crystal microbalance, Polym. J. 49 (7) (2017) 543–548.
[45] Y. Shao, et al., Optical Fiber LSPR biosensor prepared by gold nanoparticle assembly on polyelectrolyte multilayer, Sensors 10 (4) (2010) 3585–3596.
[46] P.M. Bulemo, et al., Selectivity in chemiresistive gas sensors: strategies and challenges, Chem. Rev. 125 (8) (2025) 4111–4183.
[47] J.B. Brzoska, I.B. Azouz, F. Rondelez, Silanization of solid substrates: a step toward reproducibility, Langmuir 10 (11) (1994) 4367–4373.
[48] X. Meng, D. O'Hare, S. Ladame, Surface immobilization strategies for the development of electrochemical nucleic acid sensors, Biosens. Bioelectron. 237 (2023) 115440.
[49] D. Grosso, How to exploit the full potential of the dip-coating process to better control film formation, J. Mater. Chem. 21 (43) (2011) 17033–17038.
[50] B. Timmer, W. Olthuis, A.v.d. Berg, Ammonia sensors and their applications—a review, Sens. Actuators B: Chem. 107 (2) (2005) 666–677.
[51] W. Haiss, N.T. Thanh, J. Aveyard, D.G. Fernig, Determination of size and concentration of gold nanoparticles from UV-vis spectra, Anal. Chem. 79 (11) (2007) 4215–4221.
[52] E.G. Towle, I. Ding, A.M. Peterson, Impact of molecular weight on polyelectrolyte multilayer assembly and surface properties, J. Colloid. Interface Sci. 570 (2020) 135–142.
[53] X. Lyu, A.M. Peterson, The Princess and the Pea Effect: influence of the first layer on polyelectrolyte multilayer assembly and properties, J. Colloid. Interface Sci. 502 (2017) 165–171.
[54] H. Fu, et al., Zinc oxide nanoparticle incorporated graphene oxide as sensing coating for interferometric optical microfiber for ammonia gas detection, Sens. Actuators B: Chem. 254 (2018) 239–247.
[55] S. Thaneerat, et al., Gold-coated ZnO nanostructures on no-core optical fiber for ammonia detection in food spoilage applications, Sci. Rep. 15 (1) (2025) 31030.
[56] N. Wang, et al., Polyacrylic acid/polyaniline-coated multimode interferometer for ammonia detection, Materials 16 (4) (2023) 1478.
[57] R. Kanawade, et al., Fiber optic Fabry–Perot interferometer sensor: an efficient and fast approach for ammonia gas sensing, J. Opt. Soc. Am. B 36 (3) (2019) 684–689.
[58] X. Fan, et al., Ammonia gas sensor based on graphene oxide-coated mach-zehnder interferometer with hybrid Fiber structure, Sensors 21 (11) (2021) 3886.
[59] M. Ansari, M.K. Moravvej-Farshi, Dual-purpose optical fiber sensor: relative humidity and ammonia detection, Opt. Contin. 1 (2) (2022) 335–344.
[60] H. Fu, et al., Fe2O3 nanotube coating micro-fiber interferometer for ammonia detection, Sens. Actuators B: Chem. 303 (2020) 127186.
[61] L. Li, et al., Graphene/polyaniline film optical Fiber ammonia gas sensor with excellent sensing performance, IEEE Sens. J. 23 (14) (2023) 15652–15659.